Structural Engineering and Mechanics, *Vol. 74, No. 5 (2020) 589-600*
DOI: https://doi.org/10.12989/sem.2020.74.5.589

Bond-slip constitutive model of concrete to cement-asphalt mortar interface for slab track structure

Miao Su*[1,2], Gonglian Dai[3a] and Hui Peng[1b]

[1]*School of Civil Engineering, Changsha University of Science and Technology, NO. 960, Wanjiali South Road, Changsha 410114, China*
[2]*Department of Civil and Environmental Engineering, University of California, Berkeley, CA 94720 USA*
[3]*School of Civil Engineering, Central South University, NO. 68, Shaoshan South Road, Changsha 410075, China*

(Received January 17, 2019, Revised August 19, 2019, Accepted January 10, 2020)

Abstract. The bonding interface of the concrete slab track and cement-asphalt mortar layer plays an important role in transferring load and restraining the track slab's deformation for slab track structures without concrete bollards in high-speed railway. However, the interfacial bond-slip behavior is seldom considered in the structural analysis; no credible constitutive model has been presented until now. Elaborating the field tests of concrete to cement-asphalt mortar interface subjected to longitudinal and transverse shear loads, this paper revealed its bond capacity and failure characteristics. Interfacial fractures all happen on the contact surface of the concrete track slab and mortar-layer in the experiments. Aiming at this failure mechanism, an interfacial mechanical model that employed the bilinear local bond-slip law was established. Then, the interfacial shear stresses of different loading stages and the load-displacement response were derived. By ensuring that the theoretical load-displacement curve is consistent with the experiment result, an interfacial bond-slip constitutive model including its the corresponding parameters was proposed in this paper. Additionally, a finite element model was used to validate this constitutive model further. The constitutive model presented in this paper can be used to describe the real interfacial bonding effect of slab track structures with similar materials under shear loads.

Keywords: bond-slip model; interface; push-shear test, concrete; cement-asphalt mortar; slab track

1. Introduction

With the advantages of low weight, low structure height, convenient maintenance and industrialized manufacture, slab track has been widely used in the high-speed railway all over the world (Zhu 2008). The ordinary slab track consists of the rail, fastener, prefabricated concrete track slab, cement-asphalt mortar layer, concrete bollard, and concrete roadbed (He 2005). As an important component of the slab track, the concrete bollard's main function is to restrict the longitudinal and transverse displacement of the track slab (Li 2017). The cement-asphalt mortar (CA mortar), the main material of the filling-layer for slab track, is required to have appropriate fluidity so as to fill the gap between track slabs and concrete roadbeds (Dai, Su and Chen, 2016, Dai et al. 2017). After the CA mortar is solidified, it should have enough strength and proper elasticity (Yuan et al. 2016). Moreover, for the slab track without concrete bollards, such as the Bögl slab track system in Germany (Esveld 2001) and China Railway Track System II (CRTS II) track structure (Chinese code TB10621-2014), the deformation of track slab is restrained by the interfacial bonding strength between the track slab and CA mortar layer. It is generally accepted that this interface is in a perfect bond condition and the interfacial bond-slip characteristics are ignored (China Academy of Railway Sciences 2008) in previous design of slab track. However, in the actual operation of slab tracks without concrete bollards in Chinese HSRs, the track slab to CA mortar layer interface debonding and the track slab sliding along the longitudinal or transverse directions occurred (Wang, Xu and Chen 2014). This debonding failure affects the rail's position and brings safety risks to the high-speed train's normal operation.

Among the present few researches on interfacial bond strength of slab tracks, the push-shear field-test, which can reflect the CA mortar's real interfacial bond condition, is an effective experiment study. In 2003, German Bögl Company conducted a push-shear test on the contact surface between tack slab and CA mortar layer in Neumark (China Academy of Railway Sciences 2008). The goal of this experiment is to investigate how the concrete track slab's sliding resistance is determined by the interfacial connection. In the test, two jacks were placed side by side between two track slabs to apply the shear force on the interface of the track slab and mortar layer. The load and displacement were monitored respectively. In this experiment, the interface began to crack when the load reached 410 kN, and the corresponding interface displacement was about 0.25mm to 0.45 mm. In 2012, Liu (2012) carried out a similar experiment in Suzhou, China where six specimens were tested in total. The experimental materials of CA mortar and the concrete track slabs were

*Corresponding author, Ph.D., Assistant Professor
E-mail: sumiao@csust.edu.cn; miaosu@berkeley.edu
[a] Ph.D., Professor
E-mail: daigong@vip.sina.com
[b] Ph.D., Professor
E-mail: anchor1210@126.com

ISSN: 1225-4568 (Print), 1598-6217 (Online)

the same with slab tracks in the Beijing-Shanghai HSR, but the tested longitudinal ultimate shear loads between specimens in this test are quite scattered, about 600 kN ~ 1744 kN. Besides, the damage positions of some specimens did not occur on the contact surface between track slab and CA mortar. The rest of researches on the interfacial bond strength for slab tracks are small-scale tests which were conducted in laboratories (Liu et al. 2017). Due to not considering the influences of the construction procedures of CA mortar on the interfacial bond strength, the test results measured by these laboratory tests are much larger than that of the practical slab track structure in HSR.

Although few researches studied the constitutive model of concrete to CA mortar interface, studies of other interfaces such as the concrete-FRP interface (Yuan et al. 2012, Lin and Zhang 2013, Deng et al. 2016), concrete-steel interface (Papastergiou and Lebet 2014) and laminated plates (Daouadji, Chedad and Adim 2016) can provide references for this paper. In general, there are three methods to obtain the bond-slip constitutive relationship for these interfaces: (1) Setting up a series of strain gauges on the adherend surface along the bond length direction, the interfacial shear stresses are obtained according to the differences of the two adjacent strain gauges values. The interface slip is obtained through a displacement meter at a fixed position and the superposition calculations of strain gauges values (Zheng, Huang and Han, 2014). Then the interface bond-slip relationship curves are obtained directly. The disadvantage of this method is that the measured interfacial shear stresses are discontinuous as the strain gauges cannot been arranged very closely. Besides, the accuracy of stain gauges cannot meet the experimental requirements if the interfacial strength is very weak. (2) A double cantilever beam (DCB) test (Ji, Ouyang and Li 2013) and an end notched (ENF) test (Ouyang and Li 2009) are used to measure the Mode I and Mode II interlaminar fracture toughness and interfacial strength, respectively. In these tests, the interface separation δ and energy release rate J can be experimentally determined (Monfared 2017). Then, according to the fracture mechanics theory, the interfacial shear stress can be obtained, as shown in Eq. (1).

$$\tau(\delta) = \frac{\partial J(\delta)}{\partial \delta} \tag{1}$$

Yet this method is only suitable for standard specimens (DCB or ENF specimens) instead of the push-shear field-test. (3) The interface bond-slip law can be obtained by driving and analysing the load-displacement curve at the loading end. Yuan et al. (2004) and Gao et al. (2012) have proved that the experimental load-displacement responses can be used to quantify the parameters of interfacial bond-slip relationship when the interface stress distribution in the debonding process has been studied. This method was adopted in this paper.

This paper introduces the push-shear tests of slab track's interlaminar interface and presents the load-displacement curves of typical specimens under the longitudinal and transverse shear loads. Based on the local displacement monitor system, the deformations of CA mortar as well as the interface failure mode have been obtained. The interfacial mechanical model with its governing equation of displacement, aiming at the push-shear test, was established according to theoretical analysis. By employing a bilinear bond-slip law, expressions of the interfacial shear stresses in different loading stages were derived as well. Afterwards, the theoretical load-displacement response for the interface was obtained. Finally, by ensuring that the theoretical results are consistent with the experiment results, the determination method of parameters for the bond-slip law was proposed. In addition, a finite element model was established to verify the correctness of the presented constitutive model. The goal of this research is to propose a bond-slip constitutive model for the interface of the concrete track slab and CA mortar that can reflect the real interfacial bonding effect of slab track structures in the action of shear loads.

Table 1 Parameters of the specimen

Member	Parameter	Value (mm)
track slab	length	6450
	width	2550
	thickness	200
CA mortar	length	6450
	width	2550
	thickness	30
base plate	length	/
	width	/
	thickness	500

2. Experiments

2.1 Specimens

The dimensions, materials, and construction procedure of the specimens are the same with the continuous slab track structure (i.e., the CRTS II track) in Chinese HSRs. Each specimen includes the concrete track slab, CA mortar layer, and concrete base plate from top to bottom. The detailed manufacturing dimensions of the specimens are listed in Table 1. The reaction force wall is 1.2 m high and forms an integral platform combined with the base plate so that the platform will not have displacement in the test processes due to its large stiffness.

The 28-day compressive strength of concrete of track slab and base plate were equal to 55 and 50 MPa, respectively. The flexural strength, compressive strength, and elastic modulus of CA mortar were equal to 3.5, 18.0, and 8500 MPa.

2.2 Experiment procedure

The push-shear test of the interfacial bond capacity for slab track was conducted in Shanghai-Kunming HSR, which has been described by Dai and Su (2016). The test was aim to study the interfacial bond capacity of CA

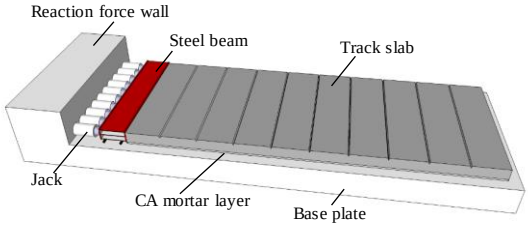

(a) Longitudinal shear test

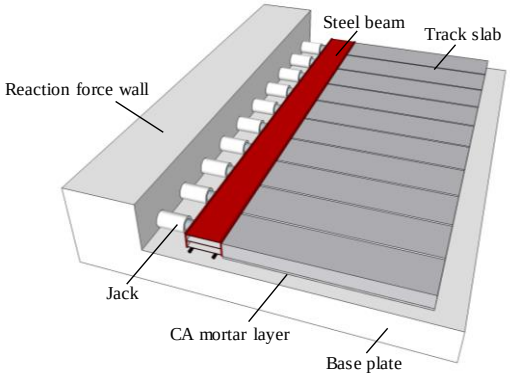

(b) Transverse shear test

Fig. 1 Experiment setup for push-shear test

mortar in longitudinal and transverse directions. In total, seven specimens (Specimen L-1 to L-7) subjected to longitudinal shear load and four specimens (Specimen T-1 to T-4) subjected to transverse shear load were completed in this experiment. The numbering of the specimen are illustrated by Specimen L-1 and Specimen T-1, where "L" means longitudinal shear test, "T" means transverse shear test, and "-1" denotes that the first specimen of the same geometrical size. The dimensions, materials, and manufacture processes of each specimen are identical.

Fig. 1 shows the experimental setups of the push-shear test in longitudinal direction and transverse direction. In the two tests, the jacks were placed on the short side and long side of the track slab, respectively. In order to make sure the hydraulic press applied from the jacks can be converted into uniform load on the cross-section of the track slab, a steel beam was attached closely in front of it. The loading system is composed of 10 jacks, in front of which 10 pressure transducers were attached to detect the load. Hence, the total load of this experiment is equal to their summation. The relative displacement between the concrete track slab and base plate was measured by LVDTs (Linear Variable Differential Transformer) whose measuring accuracy is 0.001 mm. The load and displacement were collected synchronously with a frequency of 50 Hz.

CCD (Charge Coupled Devices) cameras with 130 megapixels resolution were used to measure the local displacement of the interface. Combined with the telecentric camera lens, the measuring range of 5 mm × 4 mm and measuring accuracy of 0.001 mm can be achieved. As shown in Fig. 2, two pottery thin plates were respectively pasted on the bottom of the track slab and the top of the CA mortar layer at the loading end. For each pottery plate, a mark dot with the diameter of 0.001 mm has been manufactured on it in advance, as illustrated in Fig. 3.

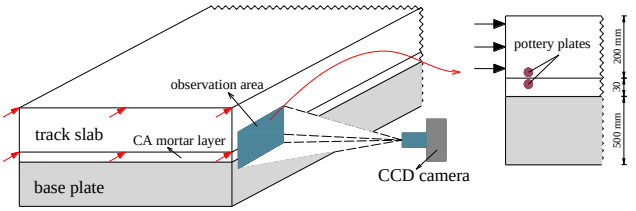

Fig. 2 CCD displacement monitor system

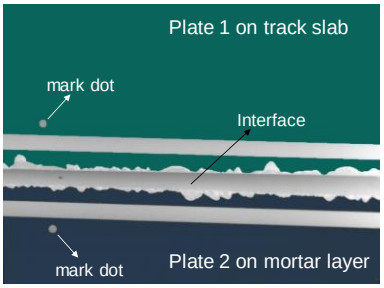

Fig. 3 Pottery plates with mark dots

Table 2 Summary of the interface shear test results

Experiments	Specimens	Ultimate load Pcr (kN)	Displacement Δcr (mm)
Longitudinal shear test	L-1	178.36	0.273
	L-2	186.46	0.547
	L-3	154.74	0.175
	L-4	166.95	0.175
	L-5	235.20	0.224
	L-6	174.44	0.078
	L-7	175.42	0.409
Transverse shear test	T-1	184.44	0.047
	T-2	172.18	0.083
	T-3	157.09	0.240
	T-4	188.16	0.233
Average value		179.40	0.225

Approximately 30,000 to 50,000 images (the sampling frequency is about 30 Hz.) of the pottery plates including mark dots are to be collected during the experiment for each specimen. After that by using the software of image calibration and computer vision technology, the positions of mark dots are determined. Hence, the motion trail curves of the dots throughout the experiment are obtained. The changes of the positions represent the displacement of the adherend (i.e., the track slab) and the adhesive (i.e., the CA mortar layer). Applying this displacement monitor system to the push-shear test, the in-plane displacement vectors of the adherend and the adhesive are obtained at the same time. The displacement vector can be eventually respectively decomposed to the displacements along and perpendicular to the loading direction.

2.3 Experiment results

Fig. 4 depicts the load-displacement curves of the specimen L-1 and the specimen T-1 that were subjected to the longitudinal and transverse shear load, respectively,

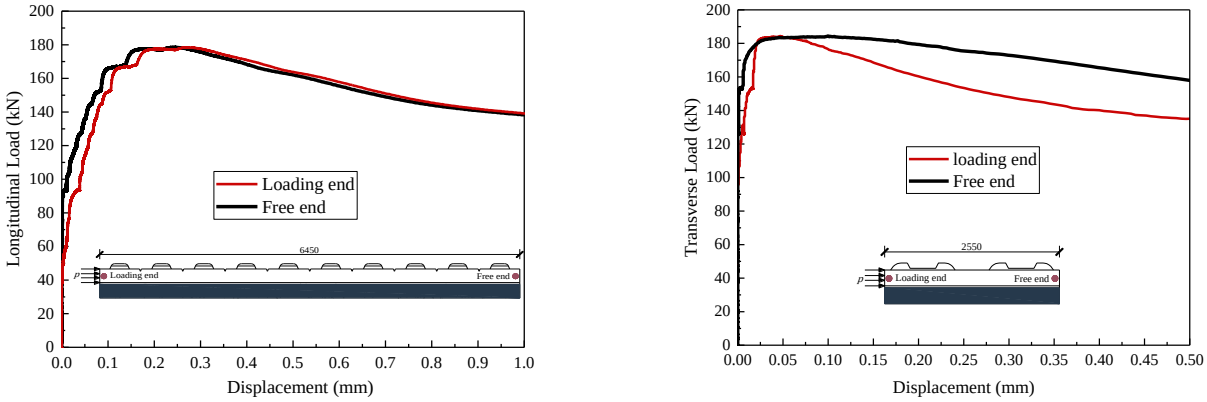

(a) Longitudinal shear test (L-1) (b) Transverse shear test (T-1)

Fig. 4 Load-displacement curves

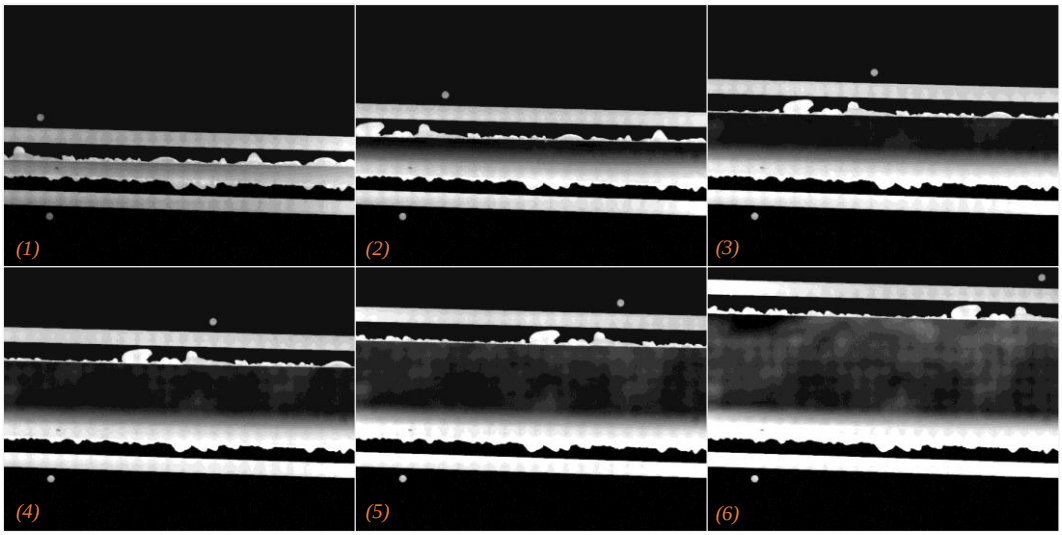

Fig. 5 Figures captured by CCD camera

in which the global displacements shown in the figure were measured by LVDTs at the loading end and free end. The ultimate bond capacities measured for these two specimens were 178.36 kN and 184.44 kN. Test results of other specimens including the ultimate load and corresponding interfacial displacement at the loading end are listed in Table 2. It can be found that the interfacial shear capacities in longitudinal and transverse directions are similar, while the average value of the ultimate load and corresponding global displacement at loading end of all specimens are 179.40 kN and 0.225 mm.

It is worth mentioning that the failure positions are at the interface of the track slab and CA mortar layer for each specimen during the experiment. After the interface cracks, only the friction resistance is remained between the contact surface of the track slab and CA mortar layer. The test results show that the friction resistance is similar to the weight of the prefabricated track slab (about 93 kN), and the interfacial slip is about 0.9 mm to 1.5 mm when the load drops to the friction force. Due to the limitation of the measurement range of LVDTs, the descending branch of the load-displacement curves measured did not reach the friction force. For the transverse shear test results shown in Fig.4 (b), as the track slab has a certain rotation after the interface bond failure, the load-displacements at loading end and free end did not coincide.

Fig. 5 shows some typical images which were captured in the push-shear test of specimen L-1. It can be seen from the figure that the mark dot on the bottom of track slab moved forward and upward gradually, while the mark dot on the top of CA mortar almost kept still. Besides, the gap between the two pottery plates became wider, which implied that the interface crack formed and expanded.

The motion trail of the mark dots on track slab and CA mortar are shown in Fig. 6, in which the x-axis and y-axis represent longitudinal (along the loading direction) and vertical displacement (perpendicular to the loading direction), respectively. It can be found in Fig. 6(a) that the track slab at the loading end has obvious longitudinal and vertical displacement. The track slab has slipped 3.4 mm along the loading direction when the test was completed. However, the CA mortar layer had almost no deformation as the positions of its mark dot fluctuated within the measuring accuracy of the CCD displacement monitor system (see Fig. 6(b)). Generally, the following features of the bonding interface can be summarized based on the experiment results:

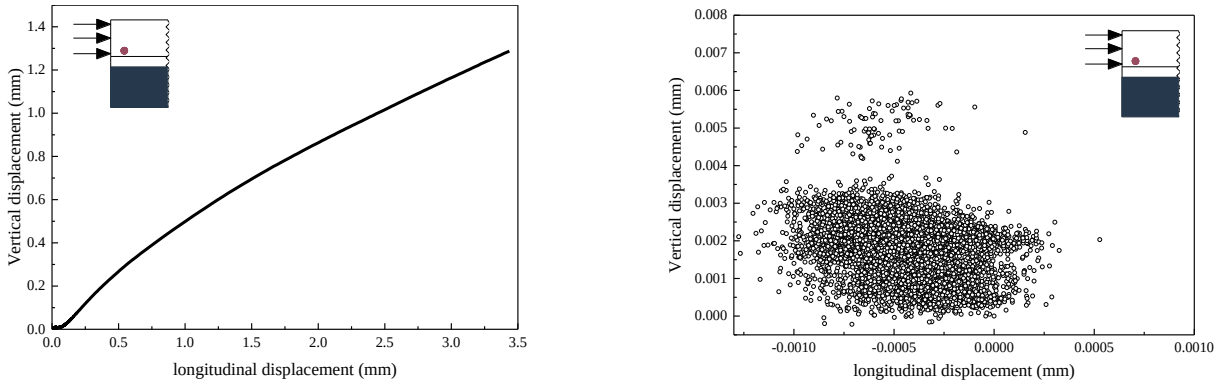

(a) Track slab (b) CA mortar layer

Fig. 6 Trajectory curves of mark dots

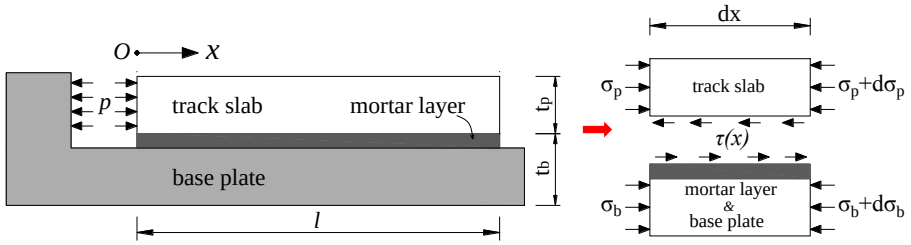

Fig. 7 Interfacial shear mechanical model for slab track structure

- There is no displacement observed or measured in the interface of CA mortar layer and base plate until the interface of the track slab and mortar layer completely fractured. Hence, the global displacement measured by LVDTs and the ultimate load can be regarded as the relative slip and the shear capacity of concrete track slab to CA mortar layer interface.
- The shear bond capacities of the interface are almost the same along the longitudinal and transverse directions.

3. Theoretical analyses

3.1 Governing equations

The interfacial mechanical model was established according to the longitudinal push-shear test, as shown in Fig. 7. The following assumptions are considered in the model:

- The CA mortar layer and the concrete base plate were considered working together as there is no interfacial displacement observed here in the experiment.
- The interface between the track slab and CA mortar layer is only subjected to shear action, in which the influences of the bending moment of the structure layers are ignored.

The width and thickness of the concrete track slab are denoted by b and t_p, respectively. While the width and thickness of the CA mortar layer and base plate are denoted by b and t_b, respectively. The length and elastic modulus of the track slab are L and E_p, respectively. Based on the equilibrium consideration of the track slab, we have

$$\sigma_p t_p - \sigma_p t_p - d\sigma_p t_p - \tau dx = 0 \tag{2}$$

$$\frac{d\sigma_p}{dx} - \frac{\tau}{t_p} = 0 \tag{3}$$

where τ is the interfacial shear stress; σ_p is the normal stress in the track slab, which can be expressed as:

$$\sigma_p = E_p \frac{du_p}{dx} \tag{4}$$

in which, u_p is the longitudinal displacement of track slab. The interfacial δ is defined as the relative displacement between the track slab and CA mortar layer, that is,

$$\delta = u_p - u_b \tag{5}$$

where u_b is the longitudinal displacement of mortar layer.

It is noted that the mortar layer's displacement u_b=0 according to test results, we thus have

$$\delta = u_p \tag{6}$$

With Eq. (6), it can be seen that,

$$\frac{d\delta^2}{dx^2} = \frac{du_p^2}{dx^2} \tag{7}$$

With Eq. (4), it can be expressed by

$$\frac{d\delta^2}{dx^2} = \frac{1}{E_p}\frac{d\sigma_p}{dx} \tag{8}$$

After substituting Eq. (3) into Eq. (8), the following equation can be derived as follows:

$$\frac{d\delta^2}{dx^2}=\frac{1}{E_p}\frac{\tau}{t_p} \tag{9}$$

The interfacial shear stress can be expressed as:

$$\tau = f(\delta) \tag{10}$$

Therefore, the constitutive equation of the interfacial displacement for slab track structure can be described by

$$\frac{d\delta^2}{dx^2}-\frac{1}{E_p t_p} f(\delta)=0 \tag{11}$$

3.2 Local bond-slip model

In the theoretical analyses, the concrete and CA mortar were considered as elastic material since they are in a low stress state. While a bilinear model illustrated in Fig. 8 that features a linear ascending branch and followed by a linear descending branch is adopted to describe the local bond-slip characteristics of the interface. This bond-slip model is mathematically described by the following:

$$f(\delta)=\begin{cases}\tau_u\cdot\dfrac{\delta}{\delta_0} & \text{when } \delta\le\delta_0\\ \tau_u+\dfrac{\tau_f-\tau_u}{\delta_f-\delta_0}(\delta-\delta_0) & \text{when } \delta_0<\delta\le\delta_f\\ \tau_f & \text{when } \delta>\delta_f\end{cases} \tag{12}$$

where τ_u is the interfacial shear strength at which the corresponding interfacial slip is denoted by δ_0, τ_f is residual shear strength after debonding due to the friction and aggregate interlock at which the corresponding interfacial slip is δ_f. As shown in Fig. 8, the bilinear bond-slip law has three segments: (a) elastic stage, when the interfacial slip $\delta < \delta_0$, the bond shear stress increases linearly with the interfacial slip until the peak shear stress τ_u (interfacial strength) is reached; (b) softening stage, when $\delta_0 < \delta \le \delta_f$, the shear stress decreases linearly with the interfacial slip; (c) slip stage, when $\delta > \delta_f$, the shear stress keeps a constant value τ_f (residual interfacial strength) with the interfacial slip.

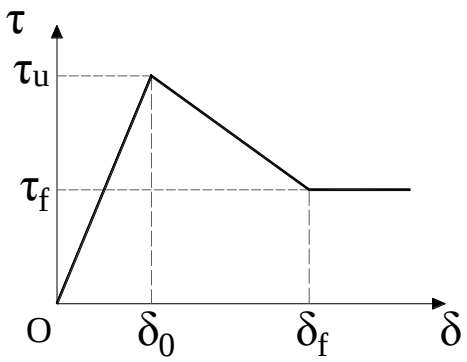

Fig. 8 Local bond-slip model

3.3 Full-range analyses of interfacial shear stress

Given that the bilinear bond-slip law defined above, the governing equation (Eq. (11)) can be solved to find the interface shear stress stage by stage during the monotonically loaded process. For the interfaces with an infinite bond length or a bond length which is substantially longer than the effective length of transferring ultimate load, Yuan et al. (2004) indicated that their debonding processes of interfacial shear stress can be divided into the elastic stage, elastic-softening stage, elastic-softening-slip stage, and softening-slip stage. In that situation, the interfacial ultimate load should be in proportion to the width of the interface. However, the push-shear tests results showed that the interfacial longitudinal ultimate load is approximately the same with the transverse ultimate load though their interfacial widths are quite different, that is, 2.55 m and 6.45 m respectively. It implies that their interfacial bond lengths of the tests (6.45 m or 2.55 m) are lower than the effective length of transferring ultimate load. Therefore, the elastic-softening-slip stage is not existed for the slab track's interlaminar interface, and its debonding processes are studied as follows:

3.3.1 Elastic stage

Firstly, when the load is small, the interfacial shear stress is less than the shear strength τ_f and it increases linearly with the interfacial slip. Substituting the relationship $f(\delta)=\tau_u\cdot\delta/\delta_0$ into Eq. (11), the following equation is obtained:

$$\frac{d^2\delta}{dx^2}-\lambda_1^2\delta=0 \tag{13}$$

where,

$$\lambda_1^2=\frac{1}{E_p t_p}\cdot\frac{\tau_u}{\delta_0} \tag{14}$$

The general solution of the differential equation Eq. (13) is

$$\delta(x)=A_1e^{-\lambda_1 x}+A_2e^{\lambda_1 x} \tag{15}$$

Then the interfacial shear stress is as follows:

$$\tau(x)=\frac{\tau_u}{\delta_0}(A_1e^{-\lambda_1 x}+A_2e^{\lambda_1 x}) \tag{16}$$

Substituting Eq. (6) and Eq. (15) into Eq. (4), the normal stress of the prefabricated slab is found by

$$\sigma_p(x)=E_p\lambda_1(-A_1e^{-\lambda_1 x}+A_2e^{\lambda_1 x}) \tag{17}$$

With the boundary conditions,

$$\sigma_p(x)=P/bt_p \quad \text{at} \quad x=0 \tag{18}$$

$$\sigma_p(x)=0 \quad \text{at} \quad x=L \tag{19}$$

where P is the external load applied on the track slab, the undetermined coefficients in Eqs. (15)–(17) can be solved:

$$A_1 = \frac{P}{bt_p E_p \lambda_1} \cdot \frac{e^{\lambda_1 L}}{(e^{-\lambda_1 L} - e^{\lambda_1 L})} \tag{20}$$

$$A_2 = \frac{P}{bt_p E_p \lambda_1} \cdot \frac{e^{-\lambda_1 L}}{(e^{-\lambda_1 L} - e^{\lambda_1 L})} \tag{21}$$

The interfacial displacement at the loading end is denoted by Δ:

$$\Delta = \delta(0) \tag{22}$$

If the Δ is already known ($0 \le \Delta \le \delta_0$), the external load can be obtained:

$$P = \Delta bt_p E_p \lambda_1 \cdot (e^{-\lambda_1 L} - e^{\lambda_1 L}) \big/ (e^{-\lambda_1 L} + e^{\lambda_1 L}) \quad \text{when } \Delta < \delta_0 \tag{23}$$

3.3.2 Elastic-softening stage

It can be found from Eq. (16) that the interfacial shear stress at the loading end reaches maximum firstly with the load increasing monotonically. Once the shear stress at the loading end (x=0) reaches τ_u, the interface commences to enter the softening stage from the loading end, while the rest of the interface near the free end remains in the elastic stage. In the softening zone, the shear stress relationship has changed to $f(\delta) = \tau_u + \frac{\tau_f - \tau_u}{\delta_f - \delta_0}(\delta - \delta_0)$. So the governing equation of the interfacial displacement for the elastic-softening stage is described as follows:

$$\begin{cases} \dfrac{d^2\delta}{dx^2} - \lambda_1^2 \delta = 0 & \text{when } 0 < \delta \le \delta_0 \\ \dfrac{d^2\delta}{dx^2} + \lambda_2^2 \delta = (\lambda_1^2 + \lambda_2^2)\delta_0 & \text{when } \delta_0 < \delta \le \delta_f \end{cases} \tag{24}$$

where,

$$\lambda_2^2 = -\frac{\tau_f - \tau_u}{(\delta_f - \delta_0) E_p t_p} \tag{25}$$

Assuming that the length of the interfacial softening zone near to the loading end is denoted by a, then, the length of the interfacial elastic zone is L–a. In the elastic zone ($a < x \le L$), the interface displacement, interface shear stress, and normal stress of the track slab are obtained like before:

$$\delta(x) = B_1 e^{-\lambda_1 x} + B_2 e^{\lambda_1 x} \tag{26}$$

$$\tau(x) = \frac{\tau_u}{\delta_0}(B_1 e^{-\lambda_1 x} + B_2 e^{\lambda_1 x}) \tag{27}$$

$$\sigma_p(x) = E_p \lambda_1 (-B_1 e^{-\lambda_1 x} + B_2 e^{\lambda_1 x}) \tag{28}$$

With the boundary conditions,

$$\delta = \delta_0 \quad \text{at} \quad x = a \tag{29}$$

$$\tau = \tau_u \quad \text{at} \quad x = a \tag{30}$$

$$\sigma_p(x) = 0 \text{ at } x = L \tag{19}$$

The undetermined coefficients in Eqs. (26)–(28) can be solved:

$$B_1 = \frac{\delta_0}{e^{-\lambda_1 a} + e^{\lambda_1 (a-2L)}} \tag{31}$$

$$B_2 = \frac{\delta_0}{e^{\lambda_1 a} + e^{\lambda_1 (2L-a)}} \tag{32}$$

While in the softening zone ($0 \le x \le a$), the solutions of the interface are given by

$$\delta(x) = C_1 \cos \lambda_2 x + C_2 \sin \lambda_2 x + \frac{\lambda_1^2 + \lambda_2^2}{\lambda_2^2} \delta_0 \tag{33}$$

$$\tau(x) = \tau_u + \frac{\tau_f - \tau_u}{\delta_f - \delta_0}[C_1 \cos \lambda_2 x + C_2 \sin \lambda_2 x + (\frac{\lambda_1}{\lambda_2})^2 \delta_0] \tag{34}$$

$$\sigma_p(x) = E_p \lambda_2 (-C_1 \sin \lambda_2 x + C_2 \cos \lambda_2 x) \tag{35}$$

With the boundary conditions,

$$\delta = \delta_0 \quad \text{at} \quad x = a \tag{29}$$

$$\tau = \tau_u \quad \text{at} \quad x = a \tag{30}$$

$$\sigma_p(x) = P \big/ bt_p \quad \text{at} \quad x = 0 \tag{18}$$

The undetermined coefficients in Eqs. (33)–(35) can be solved

$$C_1 = -\frac{\lambda_2 P \sin(\lambda_2 a) + E_p bt_p \lambda_1^2 \delta_0}{E_p bt_p \lambda_2^2 \cos(\lambda_2 a)} \tag{36}$$

$$C_2 = \frac{P}{E_p \lambda_2 bt_p} \tag{37}$$

The external load P can be obtained by integrating the shear stress on the interface:

$$P = -b[\int_0^a \tau(x)dx + \int_a^L \tau(x)dx] \tag{38}$$

in which, the shear stress $\tau(x)$ are determined by Eq. (27) and Eq. (34), respectively.

Especially, when the shear stress at the free end (x=L) reaches to the shear strength τ_u and at the loading end (x=0) does not reach the residual shear strength τ_f yet, the interface enters the complete softening stage. At this time,

$$a = L \tag{39}$$

With Eq. (33) and Eqs. (36)-(39), when the interface begins to enter the complete slip stage the interfacial slip at the loading end (which is denoted by Δs) is obtained:

$$\Delta_s = (\frac{\lambda_1^2}{\lambda_2^2 \cos(\lambda_2 L)} + \frac{\lambda_1^2}{\lambda_2^2} + 1)\delta_0 - \frac{\frac{\lambda_1^2}{\lambda_2}\delta_0 \sin(\lambda_2 L)[L + \frac{\sin(\lambda_2 L)}{\lambda_2^2 \cos(\lambda_2 L)}]}{\frac{\delta_0 - \delta_f}{\tau_f - \tau_u} E_p t_p \lambda_2^2 \cos(\lambda_2 L) + 1 - \cos(\lambda_2 L)} \tag{40}$$

With Eq. (33) and Eqs. (36)-(37), if the Δ is already known (Δ > δ_0), the external load can be expressed by

$$P = \frac{[(\frac{\lambda_1}{\lambda_2})^2 \delta_0 + \delta_0 - \Delta]E_p bt_p \lambda_2^2 \cos(\lambda_2 a) - E_p bt_p \lambda_1^2 \delta_0}{\lambda_2 \sin(\lambda_2 a)} \quad (41)$$

when $\delta_0 < \Delta \le \Delta_s$

With Eq. (38) and Eq.(41), the external load P as well as the length of softening zone a can be found by the repeated iteration.

3.3.3 Complete softening stage

When the interface is in the complete softening stage, the governing equation is described by

$$\frac{d^2\delta}{dx^2} + \lambda_2^2 \delta = (\lambda_1^2 + \lambda_2^2)\delta_0 \quad (42)$$

The solutions of the interface are given by

$$\delta(x) = D_1 \cos\lambda_2 x + D_2 \sin\lambda_2 x + \frac{\lambda_1^2 + \lambda_2^2}{\lambda_2^2}\delta_0 \quad (43)$$

$$\tau(x) = \tau_u + \frac{\tau_f - \tau_u}{\delta_f - \delta_0}[D_1 \cos\lambda_2 x + D_2 \sin\lambda_2 x + (\frac{\lambda_1}{\lambda_2})^2 \delta_0] \quad (44)$$

$$\sigma_p(x) = E_p \lambda_2 (-D_1 \sin\lambda_2 x + D_2 \cos\lambda_2 x) \quad (45)$$

With the boundary conditions,

$$\sigma_p(x) = P/bt_p \text{ at } x = 0 \quad (18)$$

$$\sigma_p(x) = 0 \text{ at } x = L \quad (19)$$

The undetermined coefficients in Eqs. (44)–(46) can be solved:

$$D_1 = \frac{P\cos(\lambda_2 L)}{E_p bt_p \lambda_2 \sin(\lambda_2 L)} \quad (46)$$

$$D_2 = \frac{P}{E_p bt_p \lambda_2} \quad (47)$$

If the Δ is already known ($\Delta_s < \Delta \le \delta_f$), the external load can be expressed by

$$P = \frac{E_p bt_p \lambda_2 \sin(\lambda_2 L)\Delta - (\frac{\lambda_1^2}{\lambda_2^2} + 1)\delta_0}{\cos(\lambda_2 L)} \quad (48)$$

3.2.4 Softening-slip stage

With the loading increasing, the shear stress at the loading end reaches τ_f and the interface enters the slip stage, while the remaining interface near the free end remains in the softening stage. Assuming that the length of the interfacial slip zone is a_d, the solutions of the interface in the range of the slip zone ($0 \le x \le a_d$) are obtained directly:

$$\tau(x) = \tau_f \quad (49)$$

$$\delta(x) = \delta_f + \frac{P - b\tau_f x}{E_p bt_p}(a_d - x) \quad (50)$$

$$\sigma_p(x) = \frac{P - b\tau_f x}{bt_p} \quad (51)$$

In the range of softening zone ($a_d < x \le L$), the interfacial governing equation is the same as Eq. (42), so the solutions of the interface are given by

$$\delta(x) = E_1 \cos\lambda_2 x + E_2 \sin\lambda_2 x + \frac{\lambda_1^2 + \lambda_2^2}{\lambda_2^2}\delta_0 \quad (52)$$

$$\tau(x) = \tau_u + \frac{\tau_f - \tau_u}{\delta_f - \delta_0}\left[E_1 \cos\lambda_2 x + E_2 \sin\lambda_2 x + (\frac{\lambda_1}{\lambda_2})^2 \delta_0\right] \quad (53)$$

$$\sigma_p(x) = E_p \lambda_2 (-E_1 \sin\lambda_2 x + E_2 \cos\lambda_2 x) \quad (54)$$

With the boundary conditions,

$$\delta = \delta_f \text{ at } x = a_d \quad (55)$$

$$\sigma_p(x) = 0 \text{ at } x = L \quad (19)$$

The undetermined coefficients in Eqs. (52)–(54) can be solved:

$$E_1 = \frac{\delta_f \cos(\lambda_2 L) - (\frac{\lambda_1^2}{\lambda_2^2} + 1)\delta_0 \cos(\lambda_2 L)}{\cos(\lambda_2 L - \lambda_2 a_d)} \quad (56)$$

$$E_2 = \frac{\delta_f \sin(\lambda_2 L) - (\frac{\lambda_1^2}{\lambda_2^2} + 1)\delta_0 \sin(\lambda_2 L)}{\cos(\lambda_2 L - \lambda_2 a_d)} \quad (57)$$

Similarly, the external load P can be obtained by integrating the shear stress on the interface:

$$P = -b[\int_0^{a_d} \tau(x)dx + \int_{a_d}^{L} \tau(x)dx] \quad (58)$$

in which, the shear stress $\tau(x)$ are determined by Eq. (49) and Eq. (53), respectively.

If the Δ is already known (Δ > δ_f), the external load can be expressed by

$$P = \frac{E_p bt_p (\Delta - \delta_f)}{a_d} \quad (59)$$

With Eq. (58) and Eq. (59), the external load P as well as the length of slip zone a_d can be found by the repeated iteration.

4. Comparisons and discussions

4.1 Comparison between experimental and theoretical results

According to the full-range analyses of the interface shear stress, it is known that the load-displacement response

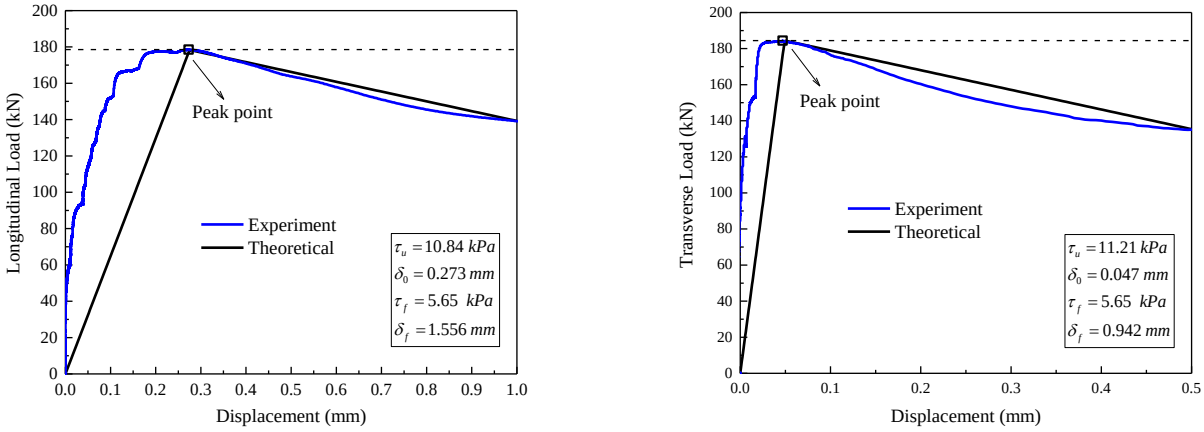

(a) Longitudinal shear test (L-1) (b) Transverse shear test (T-1)

Fig. 10 Load-displacement curves from experiment and theoretical

can be obtained once the local bond-slip law of the interface is given. In general, the interfacial constitutive parameters should be determined by iteration trial calculations with the purpose of the theoretical load-displacement curve agreeing well with the experiment results. However, the interfacial shear strength of CA mortar is weak and the bond length of the specimen is limited in this experiment, which results in that the distribution of the shear stress is relatively uniform under the action of the external load. Thus, the interfacial constitutive parameters are determined as follows: the average shear stress across the interface under the ultimate load is regarded as the interfacial shear strength τ_u (see Eq. (60)), and the corresponding displacement at loading end is regarded as the local interfacial slip δ_0 (see Eq. (61)). Similarly, the residual strength τ_f and corresponding interfacial slip δ_f are equal to the average shear stress on the interface under the friction load and the corresponding displacement at loading end, respectively (see Eqs. (62)-(63)).

$$\tau_u = P_{cr}/A \tag{60}$$

$$\delta_0 = \Delta_{cr} \tag{61}$$

$$\tau_f = P_f/A \tag{62}$$

$$\delta_f = \Delta_f \tag{63}$$

where $A = b \cdot L$ is the area of the interface.

Therefore, it can be concluded that the segment OA of the load-displacement curve shown in Fig. 9 represents the elastic stage of the interfacial shear stress; the segment AB represents the elastic-softening stage; the segment BC represents the complete softening stage; and the segment CD represents the softening-slip stage.

The geometric properties for the experiment are as follows: b = 2550 mm, t_p = 200mm, t_b = 230mm, while the elastic modulus of the concrete track slab (E_p) is 3.9×10^4 MPa, which is determined by the material performance test. Taking the specimen L-1 and the specimen T-1 as examples, the load-displacement curves obtained by experiments and

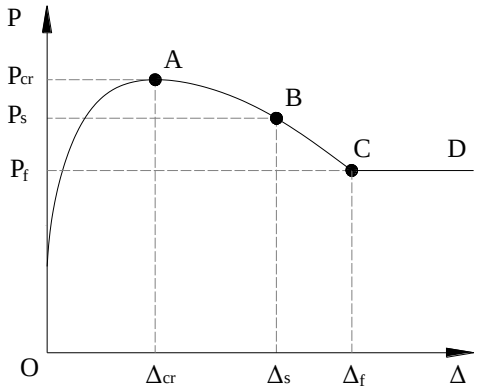

Fig. 9 Typical theoretical load-displacement curve

theoretical analyses are compared in Fig. 10. The bond-slip law parameters of the theoretical analyses in the figure are determined according to the Eqs. (60)–(63) as well as the corresponding test results of specimen L-1 and specimen T-1. It can be seen from the figure that the theoretical ultimate load and critical interfacial displacement agree well with the experiment results both for the longitudinal and transverse push-shear test. These examples demonstrate the validity of the current theoretical model in modelling the interfacial bond capacity for slab track structures.

Additionally, the interfacial shear stresses of different loading stages can also be derived according to the theoretical analyses, as shown in Fig. 11. In the analyses, the bond-slip law parameters were determined according to the specimen L-1's test results. It can be found that the shear stresses are very uniformly distributed along the bond length as the difference between the maximum shear stress and the minimum shear stress is less than 2%. Nevertheless, the shear stresses of different loading stages can be distinguished easily by the shape of the curves.

4.2 Numerical simulations

It can be found that the ascending branch of the load-displacement curve are not approached well when the bilinear interfacial bond-slip law is adopted in the theoretical analyses. Thus, the idea of replacing the bilinear

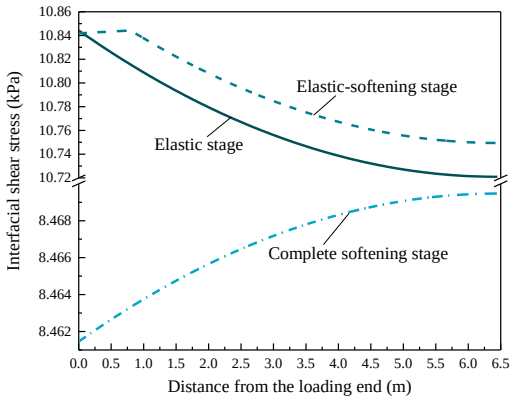

Fig. 11 Interfacial shear stresses distribution of different loading stages (L-1)

bond-slip law with the exponential nonlinear bond-slip law is considered. The linear ascending branch in Fig. 8 is changed by the following:

$$\tau = e \cdot \tau_u \frac{\delta}{\delta_0} \exp(-\frac{\delta}{\delta_0}) \quad \text{when } \delta \le \delta_0 \tag{64}$$

where e is mathematical constant and approximately equal to 2.7182. This nonlinear bond-slip law is not as simple as the bilinear relationship when to solve the equations in the theoretical analyses, but it could be adopted in the numerical simulation.

In order to validate the nonlinear bond-slip law and the presented determination method of the interfacial constitutive parameters further, the interface finite element model (FEM) of the slab track structure with the software ANSYS was established. The geometric and material properties of the model were listed in Table 3. In the FEM (as illustrated in Fig. 12), the track slab, the mortar layer, and the base plate were simulated by solid elements (Solid65); the bond-slip behavior of the interface between the track slab and mortar layer was implemented by nonlinear spring elements (Combin39) without sizes (Chen, Chen, & Teng, 2012). Both the nonlinear and bilinear bond-slip law were considered, respectively. While the coincident nodes of the interface between the mortar layer and the base plate were coupled considering there is no displacement happened here. As to the boundary conditions, the nodes of the base plate's bottom surface were restrained completely, and the external load was applied on the longitudinal or transverse cross-section of the track slab as the uniform pressure.

Table 3 Properties in finite element model

Item	Dimensions (m)	Elastic modulus (MPa)	Density (kg/m3)	Poisson's ratio
Prefabricated track slab	6.45 × 2.55 × 0.2	3.9 × 104	2600	0.3
CA mortar layer	6.45 × 2.55 × 0.03	8500	2200	0.2
Base plate	6.45 × 2.55 × 0.5	3.3 × 104	2600	0.3

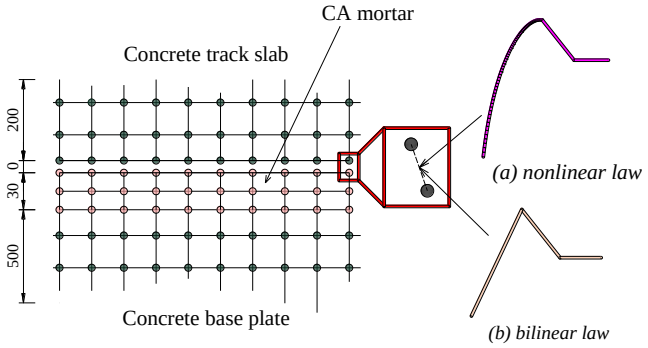

Fig. 12 FEM model and interfacial bond-slip law (unit: mm)

Table 4 Recommended interface bond-slip model parameters

Interfacial parameters	Unit	Amount	Standard deviation
τ_u	(kPa)	10.91	0.68
δ_0	(mm)	0.225	0.15
τ_f	(kPa)	5.65	0.25
δ_f	(mm)	1.200	0.35

Similarly, taking the specimen L-1 and the specimen T-1 as examples, and the interfacial parameters in FEM were determined according to the Eqs. (60)–(63). The comparisons between the experimental and FEM results are shown in Fig. 13. It shows that the load-displacement curves obtained by experiment and calculated by FEM agree well with each other whenever the load is applied along longitudinal or transverse direction. Moreover, the calculation results show that the calculated load-displacement response agree better with the experimental results if adopting this nonlinear interfacial bond-slip relationship. Therefore, the correctness of the theoretical analyses and the interfacial bond-slip constitutive parameters determination method are validated by these comparisons.

Each specimen's test results could give a set of interfacial bon-slip parameters. Considering that the experimental interfacial bond capacities are relative similar for the 11 specimens of the push-shear test, the average value of the all specimens test results can be simply regarded as the recommended interfacial bond strength parameters, as listed in Table 4.

5. Conclusions

The cohesive constitutive model and the bonding characteristics of the interface for slab track structures in Chinese high-speed railway have been investigated through experiments and theoretical analyses. The conclusions made in this paper can be summarized as follows:

- There are two bonding interfaces existed for slab track structures in high-speed railway because the cement-asphalt mortar layer has a certain thickness. The CCD local

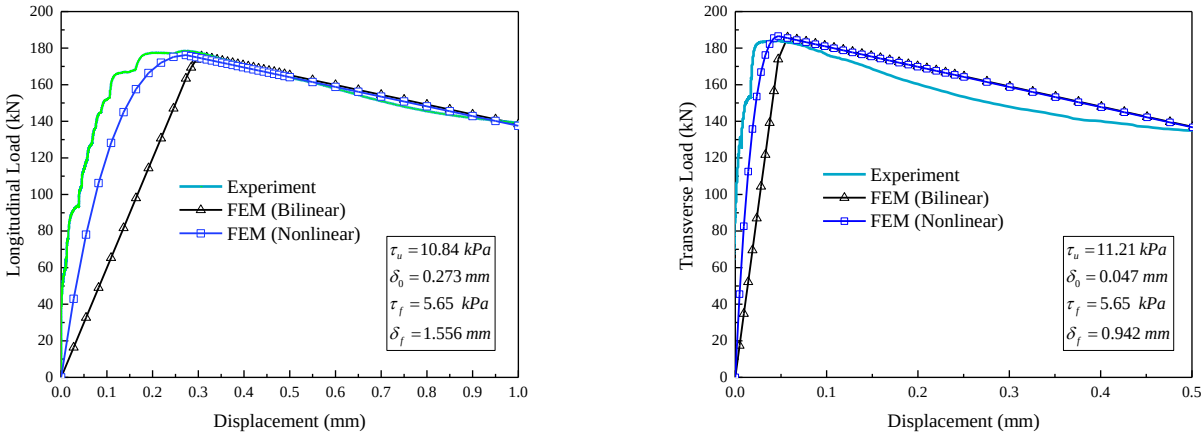

(a) Longitudinal shear test (b) Transverse shear test

Fig. 13 Load-displacement curves from experiment and FEM

displacement test results show that the bond strength of the interface between the prefabricated track slab and the mortar layer is weak and is easy to crack. It is necessary to consider its interfacial bond-slip characteristics in the design of the slab track structure. However, the bond strength of the interface between the mortar layer and the base plate is strong, which can be regarded as a perfect bonding condition.

- By establishing the interfacial mechanical model and employing the bilinear bond-slip law, the expressions for the interfacial shear stresses in different loading stages are derived. Once the local bond-slip relationship is given, the interfacial load-displacement response can be obtained through the theoretical analyses.
- Theoretical analyses show that the average value of interfacial shear stresses under the ultimate load can be regarded as the interfacial shear strength for push-shear tests since the interfacial shear stresses have a uniform distribution on the contact area. Based on the interfacial parameters determination method proposed in this paper, the theoretical load-displacement response as well as the numerical simulation results agree well with the experiment results. Additionally, replacing the bilinear bond-slip law with the nonlinear relationship in the finite element model, the calculation results can more accurately reflect the experiment, especially in the elastic stage.
- Deriving from the test results, the bond-slip model and corresponding constitutive parameters proposed in this paper can be used to describe the bond behavior of the interface of the concrete track slab and cement-asphalt mortar for slab track structures under shear loads.

Acknowledgments

The research described in this paper was financially supported by the National Natural Science Foundation of China (grant number 51808056), Research Project of Hunan Provincial Department of Education (grant number 19B012), Open Fund of National-Local Joint Laboratory of Engineering Technology for Long-term Performance enhancement of Bridges in Southern District (grant number 18KB02), and the China Scholarship Council (Grant No.201808430232).

References

Chen, G.M., Chen, J.F. and Teng, J.G. (2012), "On the finite element modelling of RC beams shear-strengthened with FRP", *Constr. Build. Mater.*, **32**(SI), 13-26. https://doi.org/10.1016/j.conbuildmat.2010.11.101.

China Academy of Railway Sciences (2008), "Summary of design principles and methods for CRTS II ballastless track of Beijing Tianjin Intercity Railway", China Academy of Railway Sciences, Beijing, China.

Dai, G.L., and Su, M. (2016), "Full-scale field experimental investigation on the interfacial shear capacity of continuous slab track structure", *Arch. Civ. Mech. Eng.*, **16**(3), 485-493. https://doi.org/10.1016/j.acme.2016.03.005.

Dai, G.L., Ge, H., Liu, W.S. and Chen, Y.F. (2017), "Interaction analysis of Continuous Slab Track (CST) on long-span continuous high-speed rail bridges", *Struct. Eng. Mech.,* **63**(6), 713-723. https://doi.org/10.12989/sem.2017.63.6.713.

Dai, G.L., Su, M., and Chen, Y.F. (2016), "Design and construction of simple beam bridges for high-speed rails in china: standardization and industrialization", *Balt. J. Road Bridge E.*, **11**(4), 274-282. https://doi.org/10.3846/bjrbe.2016.32

Daouadji, T.H., Chedad, A. and Adim, B. (2016), "interfacial stresses in RC beam bonded with a functionally graded material plate", *Struct. Eng. Mech.,* **60**(4), 693-705. https://doi.org/10.12989/sem.2016.60.4.693.

Deng, J.D., Liu, A.R., Huang, P.Y. and Zheng, X.H. (2016), "Interfacial mechanical behaviors of RC beams strengthened with FRP", *Struct. Eng. Mech.,* **58**(3), 577-596. https://doi.org/10.12989/sem.2016.58.3.577.

Esveld, C. (2001), *Modern Railway Track*, (2nd ed), Koninklijke van de Garde BV, Zaltbommel, Netherland.

Gao, W.Y., Teng, J.G. and Dai, J.G. (2012), "Effect of Temperature Variation on the Full-Range Behavior of FRP-to-Concrete Bonded Joints", *J. Compos. Constr.,* **16**(6), 671-683. https://doi.org/10.1061/(ASCE)CC.1943-5614.0000296.

He, H.W., (2005), *Ballastless Track Technology*, China Railway Publishing House, Beijing, China.

Ji, G.F., Ouyang, Z.Y. and Li, G.Q. (2013), "Effects of bondline thickness on Mode-I nonlinear interfacial fracture of laminated composites: An experimental study", *Compos. Part B-Eng.*, **47**, 1-7. https://doi.org/10.1016/j.compositesb.2012.10.048.

Li, C.N., (2017), *CRTS I Slab Ballastless Track Slab Prefabrication and Laying Technology*, China Railway Publishing House, Beijing, China.

Lin, X.S., Zhang, Y.X. (2013), "Novel composite beam element with bond-slip for nonlinear finite-element analyses of steel/FRP-reinforced concrete beams", *J. Struct. Eng.*, **139**(12), 06013003. https://doi.org/10.1061/(ASCE)ST.1943-541X.0000829.

Liu, X.Y., Su, C.G., Liu, D., Xiang, F., Gong, C. and Zhao, P.R. (2017), "Research on the bond properties between slab and CA mortar and the parameters study of cohesive model", *J. Railway Eng. Soc.*, **34**(3), 22-28.

Liu, Y. (2013), "Study on characteristics and influences of CRTS II slab track early temperature field", Ph.D. Dissertation, Southwest Jiaotong University, Chengdu.

Monfared, M.M. (2017), "Mode III SIFs for interface cracks in an FGM coating-substrate system", *Struct. Eng. Mech.,* **64**(1), 71-79. https://doi.org/0.12989/sem.2017.64.1.071.

Ouyang, Z.Y. and Li, G.Q. (2009), "Nonlinear interface shear fracture of end notched flexure specimens", *Int. J. Solids Struct.*, **46**(13), 2659-2668. https://doi.org/10.1016/j.ijsolstr.2009.02.011.

Papastergiou, D. and Lebet, J.P. (2014), "Experimental investigation and modelling of the structural behaviour of confined grouted interfaces for a new steel-concrete connection", *Eng. Struct.,* **74**, 180-192. https://doi.org/10.1016/j.engstruct.2014.05.031.

TB10621-2014 (2015), Code for Design of High Speed Railway, Ministry of Railways of the People's Republic of China; Beijing, China.

Wang, P., Xu, H. and Chen, R. (2014), "Effect of Cement Asphalt mortar debonding on dynamic properties of CRTS II slab ballastless track", *Adv. Mater. Sci. Eng.*, 193128. https://doi.org/10.1155/2014/193128.

Yuan, H., Lu, X.S., Hui, D. and Feo, L. (2012), "Studies on FRP-concrete interface with hardening and softening bond-slip law", *Compos. Struc.*, **94**(12), 3781-3792. https://doi.org/10.1016/j.compstruct.2012.06.009.

Yuan, H., Teng, J.G., Seracino, R., Wu, Z.S. and Yao, J. (2004), "Full-range behavior of FRP-to-concrete bonded joints", *Eng. Struct.*, **26**(5), 553-565. https://doi.org/10.1016/j.engstruct.2003.11.006.

Yuan, Q., Liu, W.T., Pan, Y.R., Deng, D.H. and Liu, Z.Q. (2016), "Characterization of cement asphalt mortar for slab track by dynamic mechanical thermoanalysis", *J. Mater. Civil Eng.*, **28**(3), 04015154. https://doi.org/10.1061/(ASCE)MT.1943-5533.0001401.

Zheng, X.H., Huang, P.Y., Han, Q. and Chen, G.M. (2014), "Bond behavior of interface between CFL and concrete under static and fatigue load", *Constr. Build. Mater.*, **52**, 33-41. https://doi.org/10.1016/j.conbuildmat.2013.10.080.

Zhu, G.M. (2008), "Overall comments on study and application of ballastless track at home and abroad", *J. Railway Eng. Soc.,* **7**, 28-30.